8-24-2016

MEMS-Based Terahertz Photoacoustic Chemical Sensing System

Nathan Glauvitz
Air Force Institute of Technology

Ronald A. Coutu Jr.
Marquette University, ronald.coutu@marquette.edu

Ivan R. Medvedev
Wright State University

Douglas T. Petkie
Wright State University

Published version. "MEMS-Based Terahertz Photoacoustic Chemical Sensing System," in *Progresses in Chemical Sensor* edited by Wen Wang. Rijeka,Croatia : Intech, 2016. (11-36). DOI.
Ronald A. Coutu was affiliated with the Air Force Institute of Technology at the time of publication.

Chapter 2

MEMS-Based Terahertz Photoacoustic Chemical Sensing System

Nathan Glauvitz, Ronald A. Coutu,
Ivan R. Medvedev and Douglas T. Petkie

Additional information is available at the end of the chapter

http://dx.doi.org/10.5772/62571

Abstract

Advancements in microelectromechanical system (MEMS) technology over the last several decades has been a driving force behind miniaturizing and improving sensor designs. In this work, a specialized cantilever pressure sensor was designed, modeled, and fabricated to investigate the photoacoustic (PA) response of gases to terahertz (THz) radiation under low-vacuum conditions associated with high-resolution spectroscopy. Microfabricated cantilever devices made using silicon-on-insulator (SOI) wafers were tested in a custom-built test chamber in this first ever demonstration of a cantilever-based PA chemical sensor and spectroscopy system in the THz frequency regime. The THz radiation source was amplitude modulated to excite acoustic waves in the chamber, and PA molecular spectroscopy of a gas species was performed. An optical measurement technique was used to evaluate the PA effect on the cantilever sensor; a laser beam was reflected off the cantilever tip and through an iris to a photodiode. As the cantilever movement deflected the laser beam, the beam was clipped by an iris and generated the PA signal. Experimental data indicated a predominantly linear response in signal amplitude from the photodiode measurement technique, which directly correlated to measured cantilever deflections. Using the custom-designed PA chamber and MEMS cantilever sensor, excellent low-pressure PA spectral data of methyl cyanide (CH_3CN) at 2 to 40 mTorr range has been obtained. At low chamber pressures, the sensitivity of our system was 1.97×10^{-5} cm^{-1} and had an excellent normalized noise equivalent absorption (NNEA) coefficient of 1.39×10^{-9} cm^{-1} W $Hz^{-½}$ using a 0.5 s signal averaging time.

Keywords: cantilever, MEMS, photoacoustics, spectroscopy, terahertz sensor

1. Introduction

Chemical sensing and the spectroscopic detection of chemical species can be made through various means. In this work, a direct sensing technique was performed by measuring the photoacoustic (PA) response of a microelectromechanical system (MEMS) cantilever when a gaseous sample was excited with a terahertz (THz) radiation source. The "energy deposited in the sample is measured directly" [1] through the PA effect and is proportional to the radiation source power. The PA effect was first published by Alexander Graham Bell in 1880, when he found that modulated sunlight incident on a thin disk generated sound waves [2]. Since its discovery, the PA effect has been used to study solid, liquid, and gaseous states of matter. Traditional molecular absorption spectroscopy systems measure the electromagnetic energy that is transmitted through a sample species. A disadvantage of the absorption spectroscopy technique is that it requires a baseline measurement, which is needed to account for standing waves in the system that may obscure absorption lines. In this research, the MEMS cantilever PA response to modulated THz radiation was used to investigate chemical sensing applications and collect molecular absorption spectra. An advantage over the traditional absorption spectroscopy technique is that the PA technique used here does not require a baseline measurement and it is not sensitive to baseline variations seen in traditional absorption spectroscopy techniques.

Molecules can absorb and dissipate energy through different pathways such as electronic, radiative, vibrational, and rotational pathways or through translational means via collisions [3, 4]. In recent years, many techniques have been employed for the detection of trace gases and molecular spectroscopy [1]. The PA effect is the result of molecules absorbing energy from an electromagnetic wave, where the absorbed energy is then released through collisions and other nonradiative pathways into translational energy, resulting in an increased pressure. This pressure wave can then be detected by a microphone or other pressure-sensitive device. Several different sensor methods to pick up PA waves have been implemented over the years; among them are the tuning fork [5–8], membrane microphone [9, 10], bridge [11], and cantilever designs [11–20]. As is true for any sensor configuration, the sensor design must be optimized to achieve maximum sensitivity to the anticipated changes in pressure caused by the excitation radiation captured in the PA cell.

Additional applications of MEMS and THz radiation technology have also been investigated for imaging purposes. The incorporation of superconductors [21] and metamaterials [22] on MEMS devices has enabled the direct absorption and sensing of THz radiation. As acoustic sensors, arrays of piezoelectric cantilever and spiral beam-supported diaphragm transducers have shown increased sensitivity by approximately 30 times when many transducers were connected in parallel [23]. Along those same lines, arrays of piezoelectric cantilevers have the potential to be used for THz PA imaging applications.

http://dx.doi.org/10.5772/62571

1.1. PA performance figures of merit

In PA spectroscopy and trace chemical detection systems, there are several figures of merit that are traditionally used to evaluate system performance. The first metric that must be determined is the signal-to-noise ratio (SNR). The SNR of the system is

$$SNR = \frac{PA_{Signal}}{PA_{Noise}} \tag{1}$$

where the PA_{Signal} is measured on an absorption line and the PA_{Noise} is the PA signal level evaluated in a region away from absorption lines. A high SNR is desirable because it plays a role in calculating another performance metric of the system, the sensitivity, which is described as what minimum absorption strength the system can detect. The sensitivity $\alpha_{\min}$ of a system is

$$\alpha_{\min} = \frac{\alpha_{peak}}{\mathrm{SNR}} \tag{2}$$

where α_{peak} is the strength of the measured absorption coefficient. Because PA systems can be configured differently, another useful figure of merit is the normalized noise equivalent absorption (NNEA) coefficient and it is expressed as

$$\mathrm{NNEA} = \alpha_{\min} P_o \sqrt{T}\,. \tag{3}$$

NNEA calculations allow for a better performance comparison between different PA systems by taking into account the system sensitivity, the radiation source power P_o, and the PA signal averaging time T.

1.2. PA detection systems

The PA excitation radiation source has to be specifically selected for the absorption lines of the chemical or chemicals under investigation. Radiation sources that have been commonly used are black-body sources, arc lamps, microwaves, LEDs, lasers, or tunable lasers. Kuusela et al. [12] used three different LED radiation sources, centered at 3.4, 4.2, and 7.0 μm wavelengths to excite the gaseous specimens to perform trace gas detection. Their experiment tested methane, propane, CO_2, and sulfur dioxide gases using a 3 × 1.5 × 0.01 mm^3 (length × width × thickness) silicon cantilever with a 5 μm gap around the beam. The small sensitive cantilever PA gas sensor design used a laser interferometer to measure cantilever displacement. A figure of merit for performance of a trace gas detection system can be given by the lowest achievable detection limit, which was 6 ppm for propane with a 1 s sample integration time. Experiments were performed at atmospheric pressure (760 Torr) with the gas species diluted with nitrogen to control the concentration [12].

Ledermann et al. [11] constructed a miniaturized PA cell with dimensions of approximately 15 mm in length × 8 mm in diameter to test piezoelectric acoustic sensors configured in bridge and cantilever structures for detecting CO_2 in a nitrogen-diluted mixture at atmospheric pressure. Cantilever devices were approximately 2 mm long × 2 mm wide and were fabricated using a silicon wafer that was backside etched to determine the device layer thicknesses that ranged from 5 to 20 μm. A pulsed incandescent lamp and an interference IR filter were used in the test chamber to produce 4.25 μm wavelength radiation to excite the CO_2 gas mixture. In the PA tests, depending on the CO_2 concentration, they measured 200 to 1300 μV from the piezoelectric layer on the devices, leading to a minimum sensitivity of 330 ppm CO_2 [11].

In an earlier work by Kauppinen et al. [18], a more flexible 4 × 2 × 0.005 mm^3 silicon cantilever with a 30 μm gap was used to detect methane down to 0.2 to 0.8 ppb with their PA sensor and chamber configuration. An optically chopped black-body source and a band-pass filter allowed 2.94 to 3.85 μm wavelength radiation to excite the methane gas, which has an absorption line at 3.33 μm. The methane gas tested was also diluted with nitrogen and the PA measurements were performed at a reduced pressure of 465 Torr [18].

McNaghten et al. [14] reported on an interferometer-based PA cantilever detection method that used four multiplexed tunable diode lasers at wavelengths of 1.534, 1.567, 1.568, and 1.62 μm as the radiation sources to investigate acetylene, carbon monoxide, CO_2, and methane gases in nitrogen dilution. PA measurements using a 6 × 1.5 × 0.01 mm^3 cantilever were taken on the gas samples over a range of pressures, but they found that the optimal PA signal for their system configuration was 93 Torr. Nominal data collection duration used to analyze a gaseous sample was approximately 2.62 s. To achieve the best sensitivity, signals were averaged over several minutes. The lowest NNEA for their system was achieved with acetylene gas at 1.4 × 10^{-9} cm^{-1} W $Hz^{-½}$. They evaluated the trace detection system performance over a long period of time and found that the Michelson interferometer set-up showed some instability in signal intensity over a 12 h data collection period. The fluctuations in signal intensity were attributed to acoustic noise in the room and phase shifts in the interferometer set-up seen at the photodiode [14].

Recently, Peltola et al. [17] used an interferometer-based analyzer system that included the cantilever sensor, PA chamber, and software, manufactured by Gasera Ltd. (Turku, Finland), to investigate the detection limits of hydrogen cyanide (HCN) and methane. The cantilever sensor was 5 × 1.5 × 0.01 mm^3, and Peltola et al. used a continuous-wave optical parametric oscillator (OPO) centered at ~3 μm wavelength as the radiation source. The detection limit for HCN was calculated to be 190 ppt in nitrogen and the NNEA was 1.8 × 10^{-9} cm^{-1} W $Hz^{-½}$ with an OPO power of 0.5 W and a 1 s signal averaging time. PA measurements were conducted at 300 Torr (~0.4 atm), whereas the HCN and nitrogen mixture were flowed through the chamber at ~1 L min^{-1} [17]. With another analyzer from Gasera Ltd., Sievilä et al. [19] tested six different cantilever designs in the system for PA detection, testing solid-phase materials of carbon black and polyethene. Their most sensitive cantilever design had dimensions of 5 × 1.2 × 0.005 mm^3 and a SNR = 189 while testing polyethene.

The cantilever PA systems discussed previously performed trace gas analysis to find the minimum detectable concentration of a selected gas or gases in a nitrogen-diluted environ-

http://dx.doi.org/10.5772/62571

ment. The PA measurements were conducted at reasonably high chamber pressures ranging from 93 to 760 Torr. Due to the high chamber pressures used, the PA signal was often stronger at modulation frequencies lower than the resonant frequency of the cantilever sensors. For spectroscopy applications in the THz spectral region, the PA measurements should be made at the lowest chamber pressure possible. A low chamber vacuum level minimizes the effects of pressure broadening on the absorption coefficient and allows for closely spaced absorption lines to be resolved. One of the earliest applications of THz PA spectroscopy was done by Krupnov and Burenin in the 1970s, when they constructed a submillimeter spectrometer that used a 3-μm-thick, 5 cm in diameter Mylar capacitive membrane microphone in a PA cell. They used broadband submillimeter backward wave oscillators (BWOs) as the radiation sources, which could produce frequencies of 0.199 to 1.07 THz. The chamber pressures tested ranged from 0.05 to 10 Torr and were able to achieve sensitivities of 6×10^{-9} cm^{-1} with a radiation source power of 10 mW [9].

The THz diode amplifiers used here as a radiation source for PA signal generation are modular; through different combinations of amplifier chains, the system can span 0.250 to 1.5 THz frequency range with great accuracy. The small THz PA spectroscopy system developed in this work has several advantages over traditional THz spectroscopy absorption cells. A major advantage is the reduction in size, as traditional spectroscopy absorption cells can be large, ranging from 3 to 10 ft long to increase sensitivity. Cantilever sensor designs have been shown to be more sensitive than bridge-type microphone designs [11], and the sensitive MEMS cantilever design used here enables the absorption cell size to be greatly reduced. Cantilever deflection caused by a PA pressure load dissipates the energy through bending. For a comparable membrane or bridge sensor, the deflection occurs through stretching and the devices would experience much less deflection for the same applied load conditions.

Categories for chamber pressure operating conditions have classically been divided into intrinsic, molecular, or viscous regimes [24]. Each pressure regime was named after the dominant damping mechanisms. Previously discussed cantilever PA systems were operated at higher chamber pressures of 93 to 760 Torr, which is in the portion of the pressure spectrum dominated by viscous damping effects. The molecular regime has been defined in the range of 7.5 to 750 mTorr (1–100 Pa) [24] and the intrinsic regime is defined as pressure environments less than 7.5 mTorr. A significant contribution of the research presented in this work is in the low 2 to 60 mTorr chamber pressure regimes that were investigated for the PA molecular spectroscopy applications. PA measurements in this work were performed at the lower portion of the molecular regime and just crossing over into the intrinsic damping dominant regime.

The analysis of the cantilever behavior in the PA system is first discussed through analytical equations and then finite element model (FEM) using CoventorWare® to evaluate cantilever performance. An overview of the MEMS device fabrication is then presented, which highlights the methodology used to create the cantilever PA sensor. The experimental PA test set-up is then presented, which used an extremely stable optical measurement technique to observe and record the cantilever PA signal. Cantilever dynamic behavior in the PA chamber and PA spectral data collection techniques for low-pressure environments are then presented. Finally,

the sensitivity of the system and the impact of future potential applications of this THz sensing method are discussed.

1.3. PA molecular spectroscopy

In the THz regime, molecules in a low-vacuum environment absorb energy in narrow quantized rotational states. The associated absorption frequencies are a function of the molecular structure, whereas the absorption strength depends on the electric dipole moment and structure. The characteristic absorption line shape coefficients of a molecule is subject to many different sources of line broadening, which can be established through the convolution with an appropriate broadening function. At low pressures, the dominant source of spectral line broadening is Doppler broadening, which can be represented with a Gaussian function. Doppler broadening is due to the thermal motion of the absorbing atoms, which leads to small variations in the absorbed frequency. As the chamber pressure increases, pressure broadening will play more of a role, as the absorbing molecules will collide with neighboring molecules more frequently. Pressure broadening, represented by a Lorentzian function, becomes more dominant at higher pressures. Often, spectral line widths are a function of both Doppler and pressure broadening, which can be represented through a Voigt profile and these line broadening parameters are unique to each molecule. In the THz spectral range, the optimal operating pressure is near ~10 mTorr when the Doppler broadening and pressure broadening contributions to the line shape are nearly equal.

To model the PA performance of the cantilever in the THz PA chamber, the order of magnitude of the pressure change was estimated through the use of the kinetic theory of gases and the ideal gas law. PA chamber designs can take on many different configurations such as cylindrical, Helmholtz [3], or differential [25] PA system designs. For this PA analysis, the absorption cell is assumed to have a cylindrical shape with a characteristic length l and radius r. It is also assumed that the THz radiation beam energy from the source is uniformly distributed and that the radius of the beam closely matches to that of the chamber radius. The radiation source power defined as P_o is the amount of power inserted into the chamber, whereas P is the amount of unabsorbed power that exits the chamber. Over long distances, the molecular absorption of radiation is best described by Beer's absorption law, and through a short chamber length l, the absorbed power ΔP follows the relationship:

$$\Delta P = P_o - P = P_o p_x \alpha l \tag{4}$$

where α is the absorption coefficient and p_x is the partial pressure factor of the gas under investigation. The partial pressure factor here describes the volumetric fractional abundance of the species and can be set equal to one, as no backfill of gas is used to dilute the gas species under investigation. **Figure 1** shows a segment of simulated absorption coefficient α (m^{-1}) spectra for methyl cyanide (CH_3CN) at 18 mTorr.

http://dx.doi.org/10.5772/62571

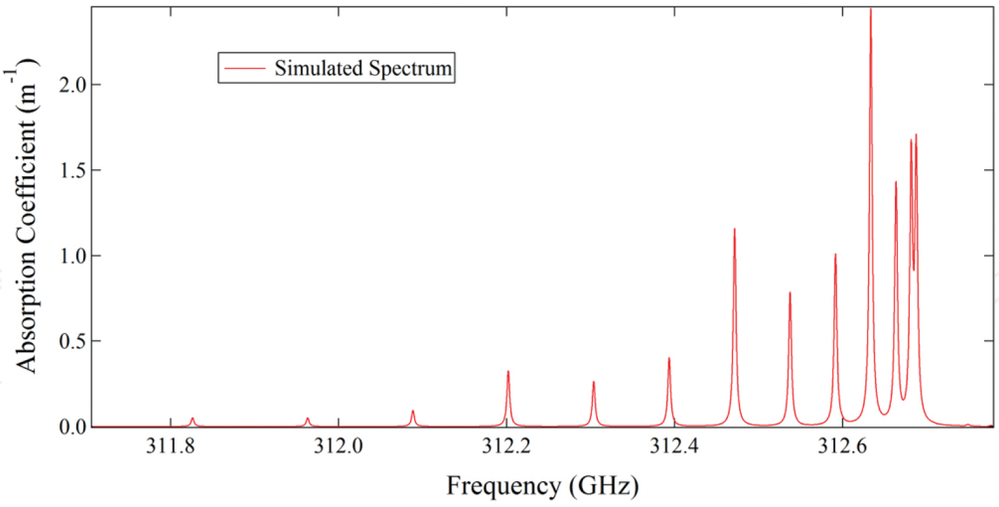

Figure 1. Small region of the simulated absorption coefficient of CH_3CN at 18 mTorr with applied pressure broadening conditions.

Based on the predicted absorption coefficients, an equation for the PA change in pressure Δp can be given as

$$\Delta p = \frac{P_o p_x \alpha l}{3 V f_m} = \frac{P_o \alpha}{3 \pi r^2 f_m} \tag{5}$$

where the anticipated change in chamber pressure per cycle as a multivariable function of radiation source power, V is the absorption chamber volume, p_x is the partial pressure factor of the gas, α is the absorption coefficient, r is the chamber radius, and f_m is the radiation modulation frequency. Based on these design space parameters, the anticipated changes in pressures could span a large range depending on the gas constituent tested and the vacuum level in the chamber. Under ideal conditions, the change in chamber pressure per cycle is expected to be approximately 18 μTorr when a radiation source power of 0.1 mW, $\alpha = 1\ m^{-1}$, $r = 5$ mm, and $f_m = 550$ Hz are used.

The sensitive microfabricated MEMS cantilever sensors created here were the key technology that significantly reduced the size of the system and enabled the low-pressure spectral measurements. A complete system integration of the sensitive MEMS cantilever sensor and the narrow line, broad spectral capabilities of the THz radiation source used with the custom low-pressure PA chamber create a uniquely powerful spectral chemical analysis tool.

2. Cantilever modeling

Cantilever motion in an under damped system can be described by Newton's second law of motion, where all the internal and external forces acting on the cantilever are set up in a detailed balance equation. The resulting differential equation describes the cantilever position based

on the forces involved and the initial conditions of the system. Of particular interest are two cases of motion, driven oscillation and damped harmonic oscillation. Using Newton's second law of motion, the equation for an under damped driven oscillator under an external driving force is represented as

$$m\frac{d^2x}{dt^2} + c\frac{dx}{dt} + kx = F\cos(\omega t + \varphi) \tag{6}$$

where m is the mass of the object, c is the damping coefficient, k is the spring constant, x is the position, dx/dt is the velocity, d^2x/dt is the acceleration, F is the amplitude of the driving force, ω is the excitation angular frequency, and φ is the phase term. A steady-state solution for displacement x for a sinusoidal applied force is

$$x(t) = A\cos(\omega t + \varphi). \tag{7}$$

The amplitude of the displacement A is a function of the modulation frequency ω, the angular resonant frequency ω_o of the cantilever and of the applied force F. When the system is modulated at the resonant frequency ($\omega = \omega_o$), the expression can be simplified to

$$A(\omega) = \frac{F}{m\sqrt{\left(\omega_o{}^2 - \omega^2\right)^2 + 4\left(\frac{1}{\tau}\right)^2\omega^2}} \cong \frac{F\tau}{2m\omega} = \frac{F}{c\omega} \tag{8}$$

where the time constant τ, defined as $\tau = 2$ m/c, represents how quickly the system dampens or responds to external stimuli. An examination of Eq. (8) reveals that decreased damping and a lower resonant frequency of the cantilever allow for the greatest amount of deflection for a given applied force.

Traditional cantilever design parameters of length, width, and thickness were used to create designs sensitive to the lower end of the anticipated pressure spectrum. As discussed above, cantilever spring constant and cantilever resonant frequencies are of great importance to the design to maximize sensitivity. An equation for the spring constant k of a rectangular cantilever beam [13] is

$$k = \frac{2}{3}E_Y w\left(\frac{h}{L}\right)^3 \tag{9}$$

http://dx.doi.org/10.5772/62571

where E_Y is the Young's modulus of the material, whereas the other parameters are the cantilever dimensions of length L, width w, and thickness h. A cantilever with the above dimensions then has a resonant frequency f_o that is then described as

$$f_o = \frac{1}{2\pi}\sqrt{\frac{k}{m_{eff}}} \tag{10}$$

where m_{eff} is the effective mass of the cantilever. Using Rayleigh's method of the conservation of energy, where ρ is the density of the cantilever material, it can be shown that the cantilever effective mass under a uniform distributed pressure load is

$$m_{eff} = \frac{104}{405}\rho whL. \tag{11}$$

Then, with these anticipated PA pressure conditions estimated through Eq. (5), potential cantilever designs were evaluated in the CoventorWare® FEM software. FEM using modal analysis of cantilever designs was performed in an earlier work and it showed that, as the cantilever width over length ratio increased, the second harmonic torsional mode frequency decreased [26]. To minimize the amount of energy dissipated through higher harmonic modes, it is advantageous to use the smaller width over length ratio cantilever designs. Using the harmonic modal analysis tool, a harmonic pressure load was applied to the surface of the cantilever as a function of frequency to find the maximum magnitude of the cantilever tip deflection. A cantilever damping parameter was used in the FEM software, defined as a fraction of the critical damping coefficient c_0, which is

$$c_0 = 2\sqrt{mk} \tag{12}$$

where m is the mass of the beam and k is the spring constant. For the simulations, the damping conditions for the analysis were set to 0.1% of the critical damping coefficient to simulate a low-pressure environment. **Figure 2** shows the tip displacement amplitude response of a 5 × 2 × 0.01 mm^3 silicon cantilever under four load conditions. Simulated sinusoidal load pressures of 0.03 to 7.5 μTorr resulted in amplitude displacements of 0.14 to 2.8 μm, respectively. The modeled results predict cantilever deflections that could easily be measured optically with a laser interferometer set-up and provided a reasonable estimate of PA performance of the cantilever design.

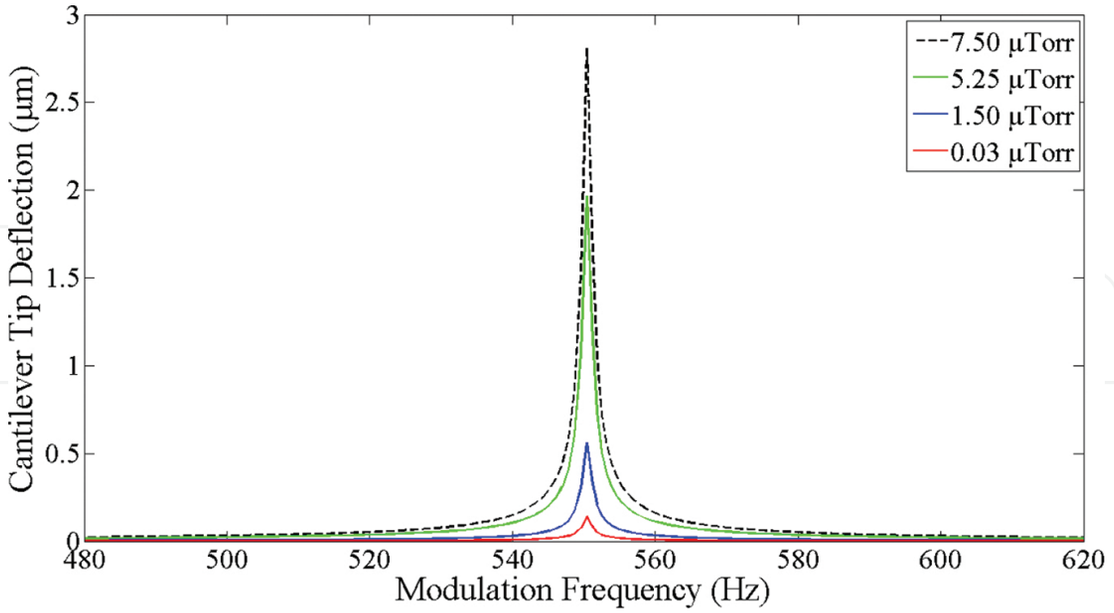

Figure 2. FEM resultant tip deflections from modal harmonic analysis of a 5 × 2 × 0.01 mm^3 silicon cantilever design under four periodic load conditions using 0.1% of the critical damping coefficient.

There are several advantages to developing an accurate FEM simulation to evaluate cantilever performance in the PA chamber. With an established framework in place, both traditional rectangular and nontraditional paddle and dual-anchor cantilever designs could be evaluated to optimize the next generation THz PA sensor. Wang et al. [27] used paddle designs out of a silicon nitride film to create airflow sensors. The paddle designs had a narrow anchor width to reduce the spring constant and a large tip surface area to capture the airflow across the sensor. Although a different cantilever design could use a dual-anchor configuration, two narrow anchor widths are spaced apart and connected to a large area to capture pressure waves. For a fixed device layer thickness, paddle and dual-anchor designs may present an advantageous means of modifying the spring constant of the beams by changing the anchor width while maintaining a larger tip surface area to capture the PA pressure.

The analysis of the analytical equations and FEM results highlights the two factors that were considered in selection of a beam design for fabrication: (1) the magnitude of the tip displacement and (2) the cantilever's resonant frequency. If the PA system is modulated at the resonant frequency of the cantilever, a higher resonant frequency would be advantageous to enable a greater number of signal averages over a short duration. A counterargument is to select a reduced resonant frequency design due to Eq. (5), which shows that the anticipated change in chamber pressure per cycle is inversely proportional to the modulation frequency, and a lower resonant frequency means a lower spring constant and therefore greater deflection. From several considered beam designs, the 5 × 2 × 0.01 mm^3 cantilever was selected for fabrication due to the predicted moderate tip deflections and resonant frequency of 550 Hz from the FEM prediction.

http://dx.doi.org/10.5772/62571

3. Device fabrication

The entire process from the initial sensor device concept design through the completed fabrication of the cantilever sensors was performed in this work. The cantilever beam designs were constructed using the device layer of Ultrasil silicon-on-insulator (SOI) (100) wafers. The selection of the SOI device layer and buried oxide (BOX) layer thicknesses were important parameters that affect both the cantilever performance characteristics and manufacturability of the devices. The BOX layer was used as an etch stop material for both the front and backside plasma etches used to create the cantilever devices.

Fabrication began with a thin layer of Ti/Au (20/100 nm) evaporated at the tip of the cantilever, which created the necessary reflective surface for the optical measurement technique employed in the experimental PA tests. A deep reactive ion etch (DRIE) plasma tool was then used to create small 3 to 8 μm gaps that were etched through the device surface of the SIO samples to define the cantilever shape. The majority of the cantilever designs fabricated in this effort were 5 × 2 × 0.01 mm^3. The advantage of using the DRIE is that it is an anisotropic etch process, which results in a near vertical sidewall profile and virtually no mask under cut to create gap widths the same resolution as the photoresist mask pattern. **Figure 3a** shows a schematic layout of the cantilever devices created and **Figure 3b** shows an optical image of a device with a small 3 μm gap achieved with the DRIE process.

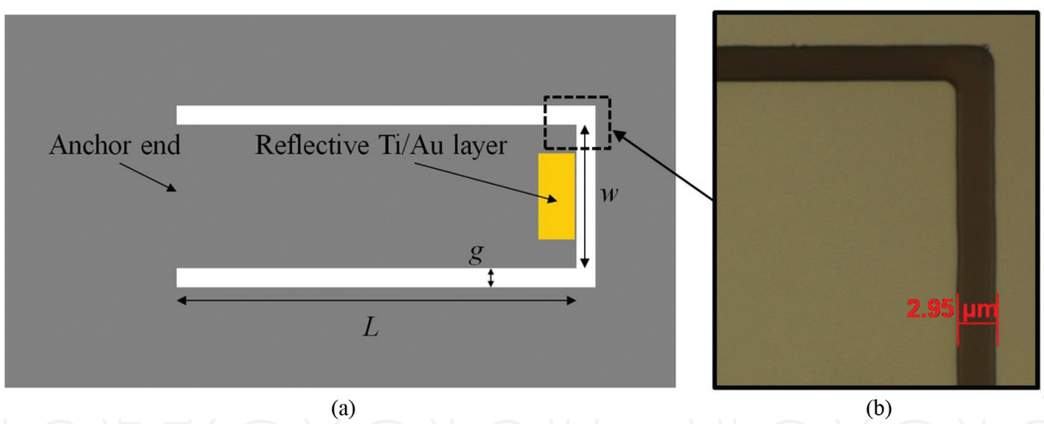

Figure 3. (a) Layout of cantilever design and (b) an optical image of the 3 μm gap etched through the device layer with the DRIE plasma tool.

To the release the cantilever beams, a hole was etched through the backside of the silicon handle wafer in a two-step DRIE and RIE process technique, which was presented in an earlier work [26]. Cantilevers fabricated here had a length/thickness ratio of 500 and a large surface area to be sensitive to the low pressures generated in the THz PA chamber. As a sensor platform, the silicon cantilever performs well, elastically deforming for small cantilever tip deflections. Due to the high length/thickness ratio of the devices, the final stages of the backside etch and cantilever release process proved to be a challenging task. The brittle nature of macroscale silicon was observed when residual stress between the device and BOX layers caused highly localized stress points, which cracked the earlier fabricated cantilever samples. These fabrica-

tion challenges were overcome through the use of a photoresist support layer [26] and a thinner 1 μm BOX layer to significantly increase the manufacturability of the high aspect ratio cantilever devices. To complete the fabrication, the BOX under the cantilever was removed with a hydrofluoric acid vapor etch. Completed devices were then tested in the custom THz PA chamber described next in the experimental set-up section.

4. Experimental set-up

The compact custom-fabricated THz PA chamber had overall dimensions of approximately 2 × 2 × 2 in^3 and was constructed out of stainless steel. The test chamber consisted of two segments: a front and back half with the cantilever sensor mounted in between them. The back portion of the chamber contained the absorption cell section, whereas the front half had a small balance volume. The absorption region portion has a cylindrical shape with dimensions of 2 in. long and a diameter of 10 mm. A schematic diagram of the back portion of the PA cell and cantilever position is shown in **Figure 4**.

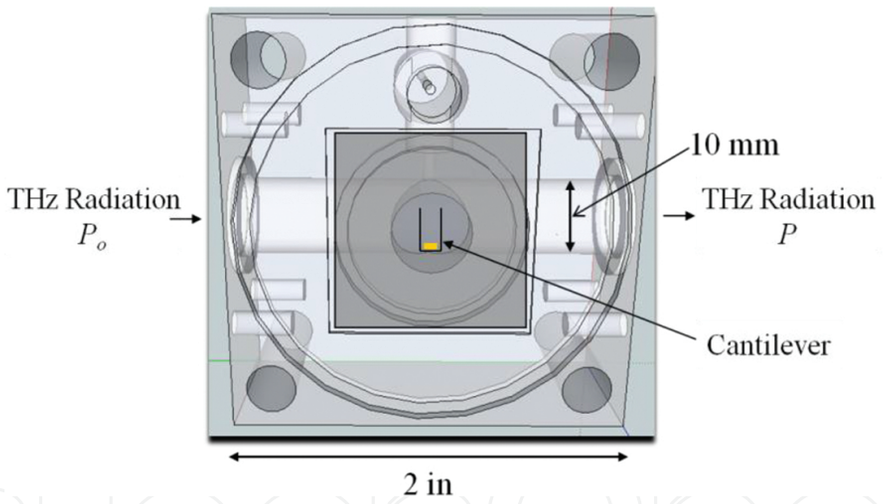

Figure 4. Schematic diagram of PA cell shown with the front portion of the chamber removed; the highlights are chamber dimensions and cantilever position in relation to the absorption cell volume.

To seal the chamber for low-vacuum conditions, Teflon windows were used to enclose the ends of the absorption cell and an antireflective (AR)-coated glass window sealed the balance volume so the optical measurements of the cantilever deflection could be made with a HeNe laser. A Pfeiffer HiCube™ turbo pumping station was used to evacuate the chamber and achieve a low base pressure vacuum level. CH_3CN, also called acetonitrile, was the first gas used to characterize the cantilever sensor. Liquid CH_3CN was exposed to the low-vacuum environment and allowed to vaporize. Through a series of valves, the CH_3CN vapor was allowed into the acoustic cell in a highly controlled manner and the absolute chamber pressure was continuously monitored with a MKS Baratron® capacitance monometer vacuum gauge.

http://dx.doi.org/10.5772/62571

PA data collection was controlled through a series of LabView VI's and the signals were collected with a National Instruments (NI) USB-6221 multifunction data acquisition (DAQ) card. To generate the THz radiation and cause the PA effect, Virginia Diodes, Inc. (VDI) amplifier multiplier chains were used. The signal to the VDI THz radiation diode was provided by an Agilent E8254A PSG-A signal generator. Controlled through the LabView interface, the output of the signal generator was set to a specified THz radiation frequency, which was then amplitude modulated on and off with a 50% duty cycle square wave at the desired modulation frequency. The emitted power by the THz VDI source ranged from 0.6 to 1.4 mW and is frequency dependent. At low chamber pressures, the output power of the THz source was too high and therefore had to be attenuated at low pressures to prevent molecular saturation. On the opposite side of the chamber from the THz source, there is a VDI detector positioned to monitor the transmitted power that exits the chamber and simultaneously measure the absorption spectra with traditional techniques. For this experiment, the amplifier chain used generated radiation over the 0.250 to 0.375 THz frequency range. An advantage to the test set-up is that additional amplifier multiplier chains can be adapted to the system to reach higher frequencies, up to 1.5 THz if required.

The PA chamber and optics for the experimental set-up were mounted on an optical bench. Two optical measurement techniques were employed to examine the PA effect. A diagram of the test set-up is shown in **Figure 5**. A HeNe (λ = 633 nm) laser beam, guided through a series of mirrors, beam splitter, irises, and focusing lens, was reflected off the tip of the cantilever, back to a photodiode where the laser beam power was measured. An iris beam clipping method or optical beam deflection method, similar to Garcia-Valenzuela and Villatoro [28], was used to collect PA spectral data in the THz test chamber when the reference mirror was blocked.

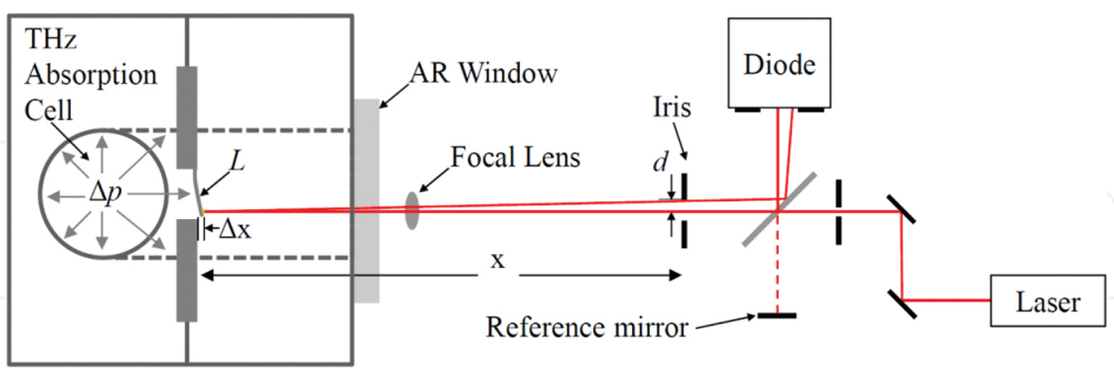

Figure 5. Diagram (not to scale) shows both the PA optical measurement techniques used; beam clipped by the iris when the reference mirror is blocked and a Michelson interferometer displacement measurement when the reference arm was used.

To quantify the sinusoidal changes in power observed at the photodiode, a Michelson interferometer measurement was also incorporated into the experiment. Switching to the interferometer measurement was accomplished by unblocking the reference mirror, modifying the filter settings of the photodiode amplifier, and removing the iris closest to the PA

chamber. Accurate cantilever tip deflections measurements were made through the generated constructive and destructive inference signal measured at the diode detector. For large cantilever deflections, the photodiode signal goes through maxima to minima interference patterns as the cantilever deflects a distance of $\lambda/4$.

In both measurement techniques, the photodiode signal was sent to a Stanford Research Systems SR560 preamplifier, set-up in a band-pass filter configuration. The photodiode signal was also sent to a Stanford Research Systems SR530 lock-in amplifier. The amplitude modulated frequency from the Agilent E8254A signal generator is used as the reference signal for the SR530 lock-in amplifier. The two-channel output of the lock-in amplifier reported the magnitude and phase components of the amplified photodiode signal compared to the reference.

For the iris beam clipping method, the measured PA signal at the diode was greatly affected by the iris placement at distance x in front of the cantilever and the positioning of the focal lens. The focal lens was positioned such that the beam formed a tight spot at the tip of the cantilever and beam spot at the detector was smaller than the detector opening. Iris placement in front of the cantilever served two purposes. The first function was to reduce the diameter of the incoming beam before the laser light impinged the cantilever. The second purpose was to act again as an aperture; light reflected off the deflected cantilever was then clipped by the iris before it reached the photodiode. The diameter of the iris closest to the chamber was set to ~0.8 mm. The final spot size of the HeNe laser beam at the photodiode was ~1.1 mm in diameter. The beam displacement d from steady state shown in **Figure 5** is expressed by

$$d = x \tan\left(\sin^{-1}\frac{\Delta x}{L}\right) \tag{13}$$

where x is the distance from the cantilever steady-state position to the iris, Δx is the cantilever deflection distance, and L is the cantilever length. To obtain the optimal signal, the THz source was modulated at the resonant frequency of the cantilever, and the chamber, mounted on a three-axis stage, was adjusted until the photodiode signal produced a symmetric amplitude sine wave. The sinusoidal peak-to-peak voltage signal from the photodiode and the magnitude of the lock-in amplifier signal were used to collect the PA spectral data from the sample gas. The peak-to-peak voltage signal created at the photodiode was due to the linear region of a three-dimensional Gaussian beam profile caused by the clipping iris when the center of the beam was shifted by a total distance of $2d$. The PA signal and interferometer measurements are discussed further in the Results section.

5. Results

The experimental results are discussed in two distinct topic areas: cantilever behavior and PA spectral data. The first important aspect to discuss is the cantilever sensor dynamic behavior

http://dx.doi.org/10.5772/62571

in response to the PA effect in the test chamber. Relevant information about the behavior of the cantilever sensor includes determining the resonant frequency, quality factor, time constants, and PA signal vs. cantilever deflection for the system over the range of tested pressures. Based on the identified cantilever sensor traits, data collection rates, techniques, and PA spectral collection results are discussed.

5.1. Cantilever sensor

To investigate the cantilever and PA chamber performance, CH_3CN was selected because it has documented absorption lines over a large spectrum (0.018–1.8065 THz), making it an ideal gas, as the radiation source can span a large portion of that spectrum. Also, CH_3CN has both strong and weak absorption line strengths within that frequency range, which would demonstrate the large dynamic range capability of the cantilever PA system. Initial PA data were taken using the absorption line frequency just over 312.633 GHz, identified as Freq 1 from here forward. Then, to acquire the optimal PA signal from the cantilever, a modulation frequency scan was performed using the THz Freq 1 absorption line. Modulation frequency scans from 1 to 700 Hz found that the maximum PA signal was achieved when the system was modulated at the resonant frequency ($\omega \cong \omega_o$) of the cantilever. **Figure 6** shows the PA signal from the lock-in amplifier as a function of modulation frequency over the 3 to 400 mTorr pressure ranges.

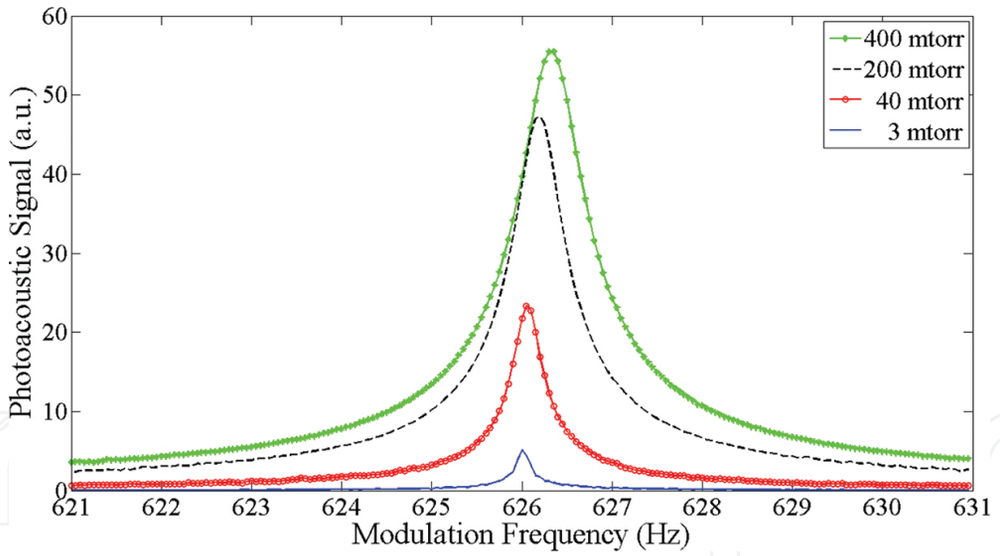

Figure 6. PA response of the cantilever as a function of modulation frequency for four different pressures tested revealed that the maximum PA signal was achieved at slightly higher modulation frequencies with increased chamber pressure.

The required modulation frequency to achieve the maximum PA signal increased nonlinearly with increasing chamber pressure, approximately 8.8×10^{-4} Hz $mTorr^{-1}$ overall. The slight observed frequency shift was attributed to an increase in the effective spring constant of the system due to the gas interactions with the cantilever, which increased as a function of chamber pressure [20]. More importantly, from the modulation frequency scans, the quality factor of

the cantilever in the low-vacuum conditions can be assessed. The quality factor of a cantilever can be expressed as

$$Q = \frac{\omega_o}{\Delta\omega} = \frac{f_o}{\Delta f} \tag{14}$$

where f_o is the resonant frequency of the cantilever and Δf is the full-width half-maximum of the PA signal. Due to the low damping conditions of the rarified gas in the PA chamber, the cantilever had a sharp resonance response to the modulation frequency scan and small Δf values of 0.15 to 1 Hz were measured. At the low vacuum pressures tested, the 5 × 2 × 0.01 mm^3 cantilever design had high-quality factors that are shown in **Figure 7**.

Using the optimal modulation frequency of the cantilever found at each pressure, the dynamics of cantilever excitation and relaxation was investigated. **Figure 8** shows a sample of PA data collected from the system at a chamber pressure of 3 mTorr using THz Freq 1. The THz excitation on time was 8 s and it can be seen in the graph that the lock-in PA signal was just approaching a steady state before the radiation was turned off. As the chamber pressure increased, the PA signal response time improved. In **Figure 9**, PA data were collected at a chamber pressure of 80 mTorr. The higher chamber pressures showed a much quicker response to reaching steady-state conditions and generated a stronger PA signal, and the output of the lock-in signal reached a steady-state value in approximately 4 s.

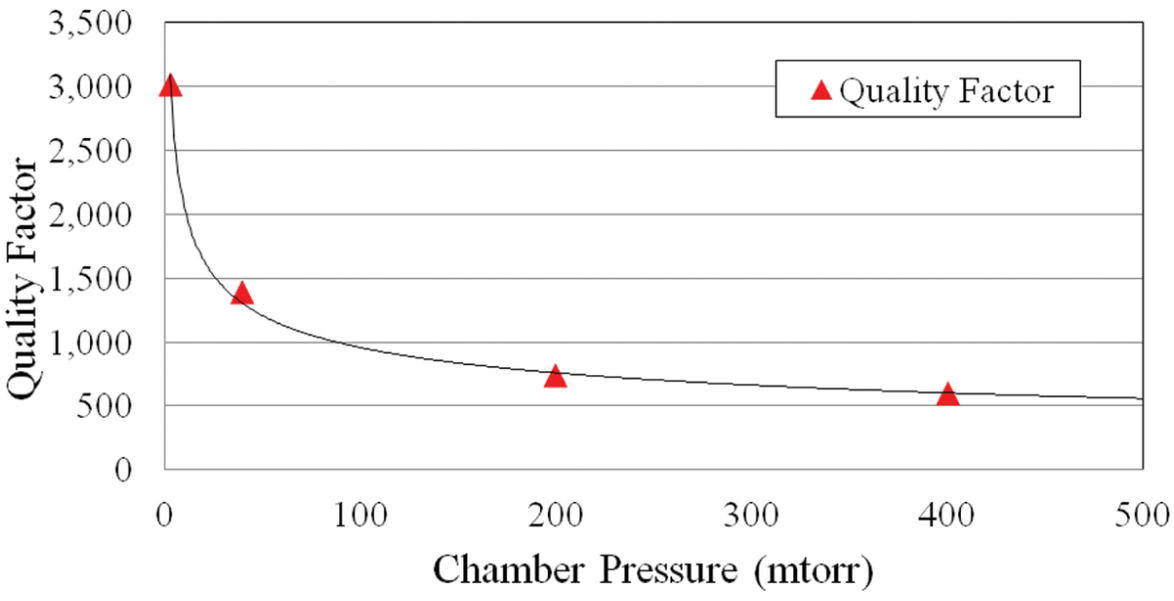

Figure 7. Quality factor of the 5 × 2 × 0.01 mm^3 cantilever sensor was high due to the low-pressure intrinsic/molecular damped environments in the PA chamber.

http://dx.doi.org/10.5772/62571

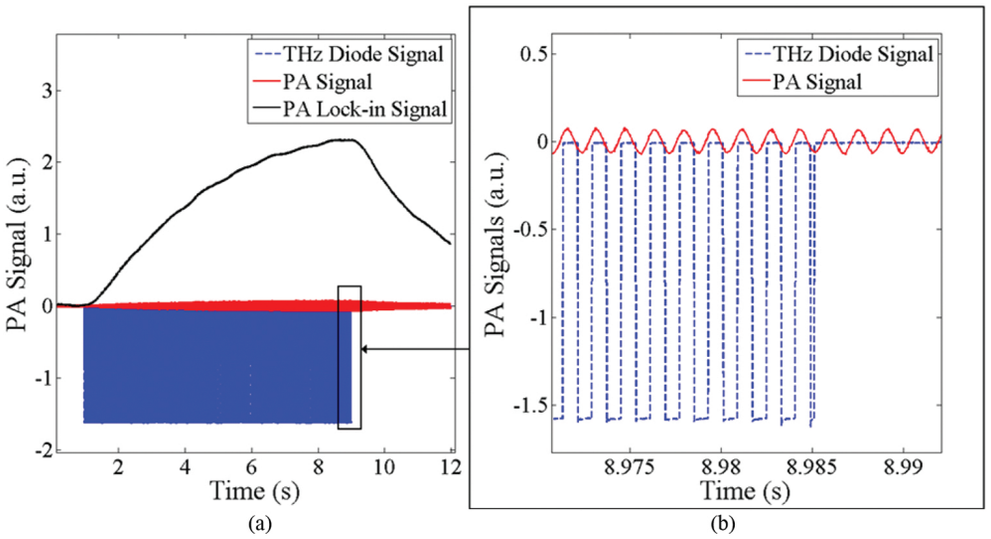

Figure 8. PA data recorded at 3 mTorr in plot (a) shows the slow response of the lock-in amplifier and raw PA signals at the low chamber pressure. Plot (b) is a zoomed-in view of the raw PA signal from the diode and modulated THz signal as the radiation is turned off.

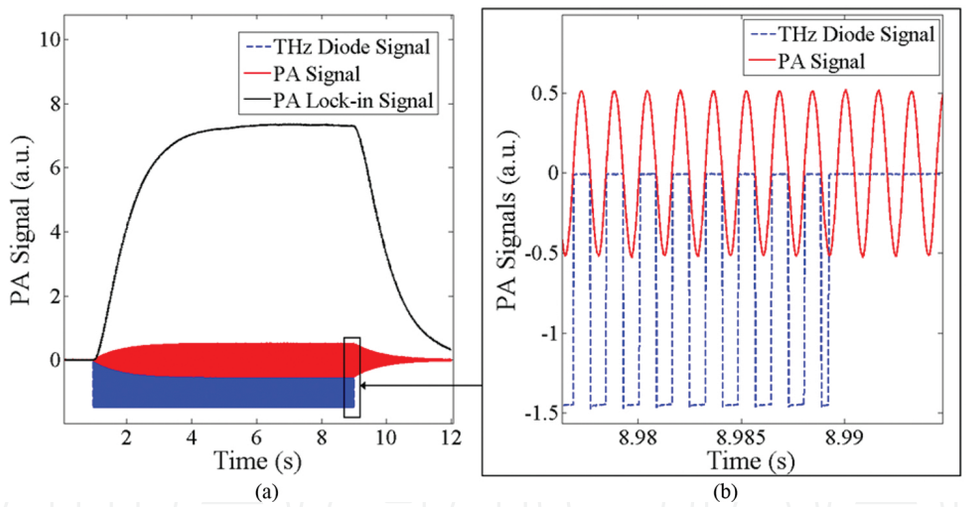

Figure 9. PA data in plot (a), taken at 80 mTorr, illustrates the quicker response time of the lock-in PA signal and raw PA signal from the THz excitation radiation at higher chamber pressure. Plot (b) is a zoomed-in view of the raw PA signal from the diode and modulated THz signal.

For a range of pressures, the cantilever was brought up at an excited state and then the exponential decay of the PA signal was recorded. An exponential curve fit was then performed on the PA data to extract the time constants, τ. The resulting time constant versus pressure plot is shown in **Figure 10**. Time constants dramatically increase as the chamber pressure gets lower and moves from the molecular to intrinsic pressure regime. For the investigated pressures, a curve fit was performed using a power function. An equation for the time constant as a function of pressure was found to be

$$\tau(p_c) = 4.553 p_c^{-0.32556} \tag{15}$$

where the chamber pressure p_c is given in mTorr. The resultant function shown in Eq. (15) had a strong correlation to the experimental measurements and had an R^2 value of 0.998. At a chamber pressure of 3 mTorr and a lock-in time constant of 0.3 s, it was found to take approximately 8 s for the PA signal from the lock-in amplifier to reach a steady-state value. This long required excitation time at lower chamber pressures can be expected due to the extremely low pressure change generated per modulation pulse.

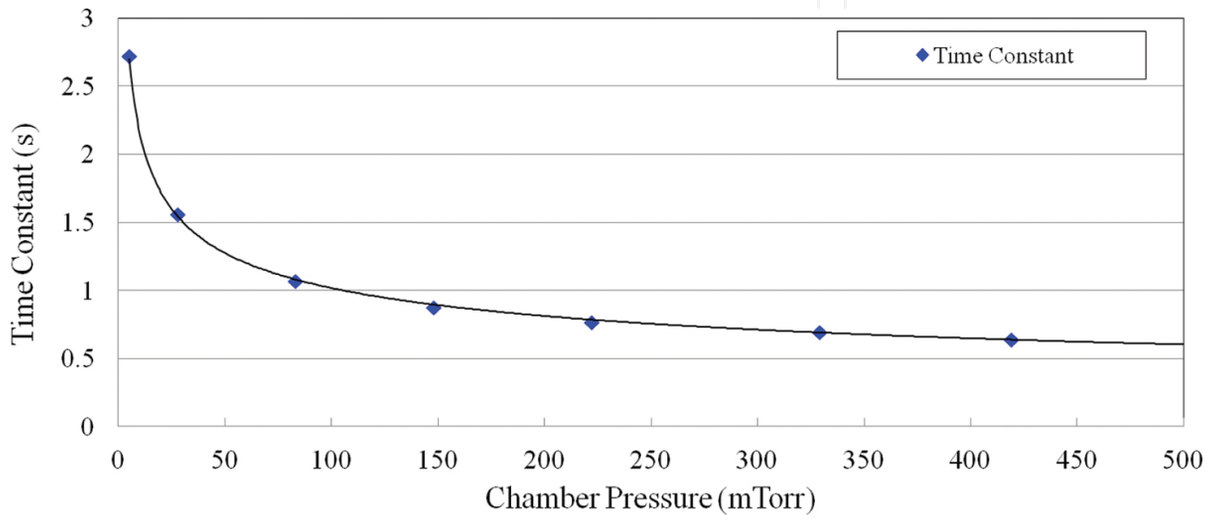

Figure 10. Time constants found through the exponential curve fit to the decay of PA signals over the range of pressures shown.

To quantify the PA signal generated by the diode voltage measurements, cantilever displacement measurements with a Michelson interferometer configuration were performed. Peak-to-peak PA signal and cantilever tip displacement measurements shown in **Figure 11** were taken across a small range of pressures. The left side of the graph corresponds to the diamond-shaped markers, which are the peak-to-peak PA signal data points. Circular data points on the graph with error bars correspond to the axis on the right, which shows the amplitude of cantilever deflection from center position given in microns. When the chamber was pumped down to a high vacuum condition, no THz PA signal could be measured. It can be seen in the graph that, as the pressure increased with the addition of CH_3CN, the measured PA signal and cantilever deflection continued to increase with pressure. Above ~7 μm deflection, the PA signal increased only slightly due to the positioning of the laser beam through the iris. This strong correlation between the PA signal and deflection measurements provides good justification for using the iris-clipped PA method for the range of deflections encountered. An additional advantage of the of the iris-clipped PA method is the modest required sampling rate; four channels of data can be digitized at 60,000 samples per second allowing for multiple channels of data to be collected simultaneously.

http://dx.doi.org/10.5772/62571

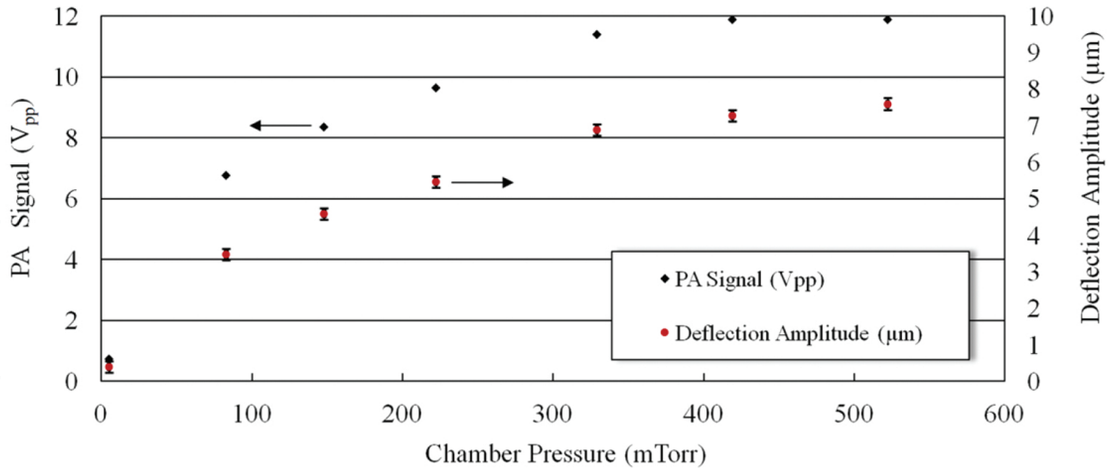

Figure 11. Graph of measurements taken on 5 × 2 × 0.01 mm^3 cantilever at different chamber pressures show PA peak-to-peak signals represented by a diamond shape corresponding to the scale on left, whereas the interferometrically measured cantilever amplitude deflections, shown with a circle and error bars, correspond to the deflection scale on the right.

The frequency spectrum of the PA system noise and an active PA signal were also investigated. In **Figure 12**, a 1 s duration of data was evaluated using Fourier analysis of the PA signal and noise. The inset in **Figure 12** shows the single-sided amplitude of the FFT when the THz source was off. With the THz source operated at Freq 1 at a modulation frequency of 626.02 Hz, the PA signal was more than 1000 times greater than the noise. The PA system had a low amount noise in the measurement signal. Two portions of the spectrum that stood out slightly were the noise signals occurring below 200 Hz and region around the resonant frequency of the cantilever. The signal around the resonant frequency of the cantilever beam was attributed to the pickup of vibrations in the experimental set-up due to noise and vibrations in the room.

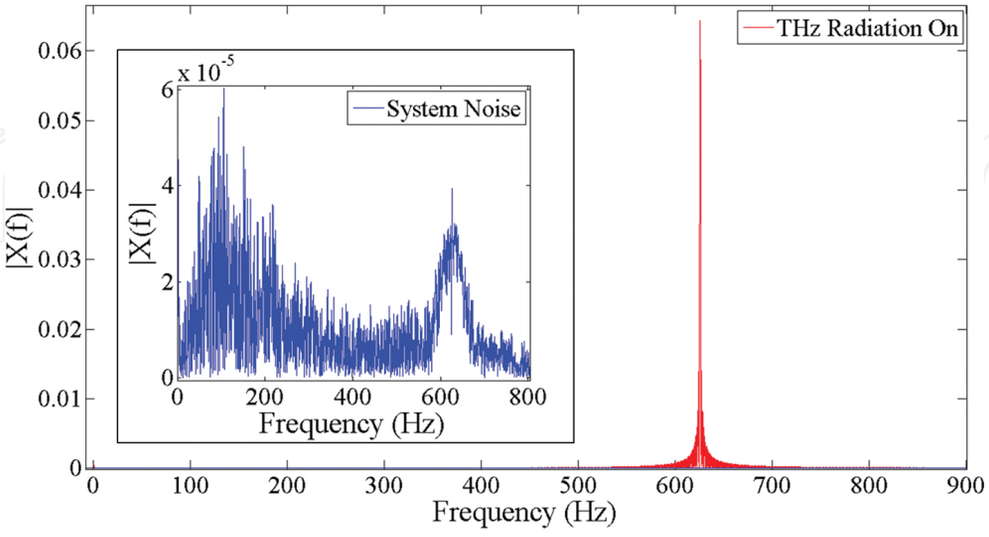

Figure 12. Fourier analysis of a 1 s PA signal, collected at 200 mTorr taken at Freq 1, showed low noise in the system with no single dominant noise frequency in the iris-clipped PA measurement method.

5.2. PA spectral analysis

PA spectral data collection was also performed across a range of pressures. As discussed earlier in the cantilever sensor analysis, chamber pressure greatly affected PA signal strength and response time. Therefore, two data collection techniques were investigated; fast scan methods to coarsely cover a broader-frequency spectrum and a slow scan method to achieve a stronger and more accurate PA signal. Spectral data collection measurements were performed in two steps: excitation and signal averaging segments. The amplitude modulated THz radiation at the specified THz frequency was turned on for a period of time, which we defined as the excitation time. This excitation time or period allowed the cantilever to attain an excited level of amplitude displacement from the generated PA pressure pulses. After the excitation time, the PA signal was averaged over the second specified interval, referred to as the signal averaging period. The PA signal measured during the signal averaging period was recorded as the PA signal for that specific THz frequency. The THz frequency was then increased by a small amount and the measurement sequence was repeated.

To show the effects of excitation time and resulting PA signal, different excitation times were performed. The signal averaging period was held constant for each of the trials and was set to a 0.1 s duration. **Figure 13** shows the results of three excitation times taken at a chamber pressure of 59 mTorr with a frequency step size of 0.05 MHz. The 2 s excitation PA spectral collection took 9.7 min, the 0.5 s excitation set took 2.8 min, and the 0.1 s excitation data set took 0.9 min to collect. The PA response shows a pronounced frequency shift at the rapid 0.1 s excitation time and a marked reduction in PA signal strength. This observed frequency shift highlights three regions of particular interest in the PA signal. First is the frequency location of the maximum PA signal, and it should ideally occur at line center frequency where the

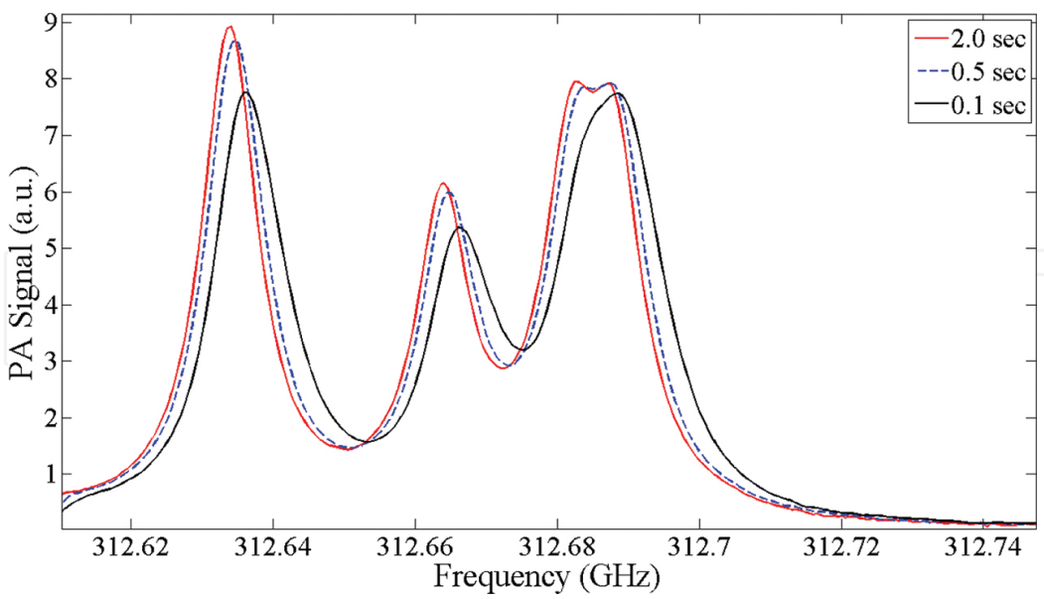

Figure 13. Spectral PA signals taken at 59 mTorr with 2, 0.5, and 0.1 s excitation times using a 0.05 MHz step size, moving from low to high frequency, the PA peak response shifted to higher frequencies and reduced amplitudes as the excitation time was decreased.

http://dx.doi.org/10.5772/62571

maximum absorption occurs. The other two important regions are the rising and the falling edge of the absorption curve about the maximum PA signal, which are due to the line broadening mechanisms mentioned earlier.

A few drawbacks exist to low-pressure (2–60 mTorr) spectral PA data collection. On the rising edge of the PA signal, PA excitation to full amplitude deflection under low-pressure conditions can take more than 4 to 12 s due to the low excitation pressure generated in the chamber and the high-quality factor of the cantilever resonator. Likewise, on the falling edge of the PA signal, once the cantilever reaches an excited steady state, the small damping coefficient at the lower chamber pressures and continued excitation at a lower absorption strength cause the amplitude of the cantilever deflection to reduce slowly, which is manifested in a small frequency shift on the downward slope of the PA signal. Radiation excitation frequency and the corresponding PA response are the crucial parameters that would be used for chemical identification applications, so they must be accurately identified.

That being said, the fast scan technique tested above is extremely useful and could be used to quickly evaluate small spectral regions for absorption lines if an unknown chemical were evaluated with the system. Then, a slower, more accurate scan could be performed to identify the line center absorption frequency and the relative PA amplitudes for each absorption line. To achieve an accurate line center absorption frequency during a spectral scan, the excitation time had to be increased as the chamber pressure decreased. At the lower 2 to 5 mTorr pressures tested, spectral line broadening appeared to be dominated by Doppler broadening effects and created the narrowest spectral line widths. As line broadening increased with pressure, the frequency step size could be increased and the excitation time could be decreased. In **Figure 14**, a small portion of spectra was recorded for three low-pressure cases. Each collection took 10 to 12 h due the small 0.05 MHz step size used and the 12

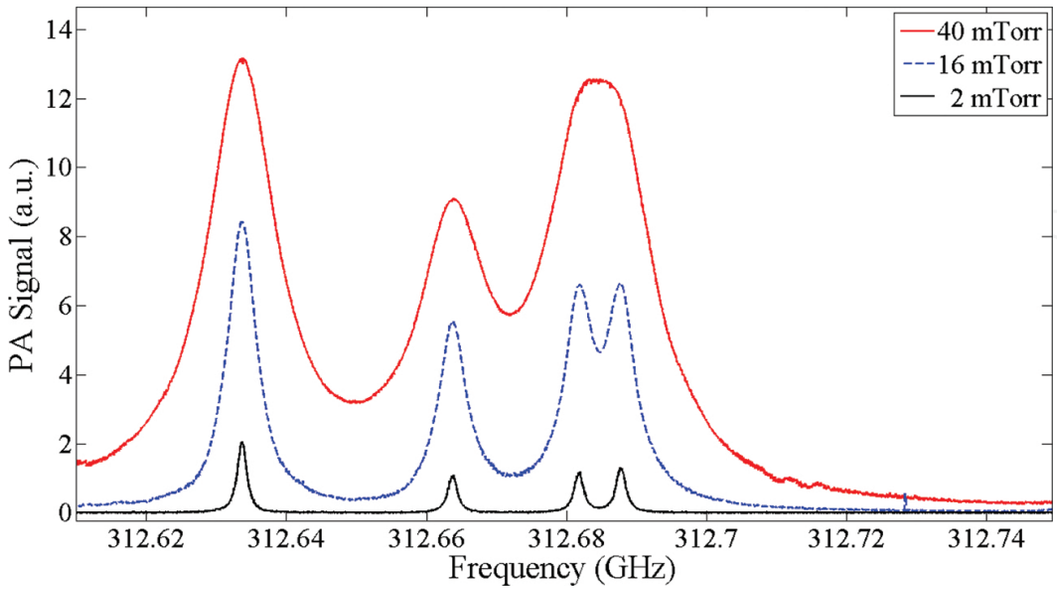

Figure 14. PA spectral data of CH_3CN collected at three pressures used a 0.05 MHz step size and recorded the 0.5 s average PA signal for each frequency step.

to 15 s excitation time before the subsequent 0.5 s average PA signal was recorded. The PA spectra presented in **Figure 14** is of interest for two reasons. This spectral region contains strong absorption lines and it also contains two peaks in close proximity, separated by only 6 MHz. The data in **Figure 14** also show the effects of pressure broadening in the PA signal as the two closely spaced absorption lines merge into one PA peak at higher chamber pressures.

During the long data collection runs, the PA measurement scheme employed for the experiment using the iris-clipped laser beam diode signal and lock-in amplifier signals proved to be extremely stable. The PA chamber maintained low vacuum levels well. Over the course of the long data collections, the chamber pressure increased slowly and had an average system leak rate of 0.5 to 1 mTorr h^{-1}.

To demonstrate the broader spectral performance of the THz PA system, a 0.72 GHz frequency scan was performed spanning 312.07 to 312.79 GHz. This low-pressure PA signal taken at 13 mTorr successfully captured the 13 rotational absorption lines in the CH_3CN spectral region scanned. The data collection method used 0.2 MHz step size and 12 s excitation, and then the 0.5 s average signal from the lock-in amplifier was recorded. This much larger PA scan of CH_3CN shown in **Figure 15** took 12.5 h to collect, and it also compares the simultaneously recorded THz diode signal to the modeled absorption coefficient profile. The scaled simulated spectra closely matched the measured PA signature of the gas with a small deviation at higher absorption strengths.

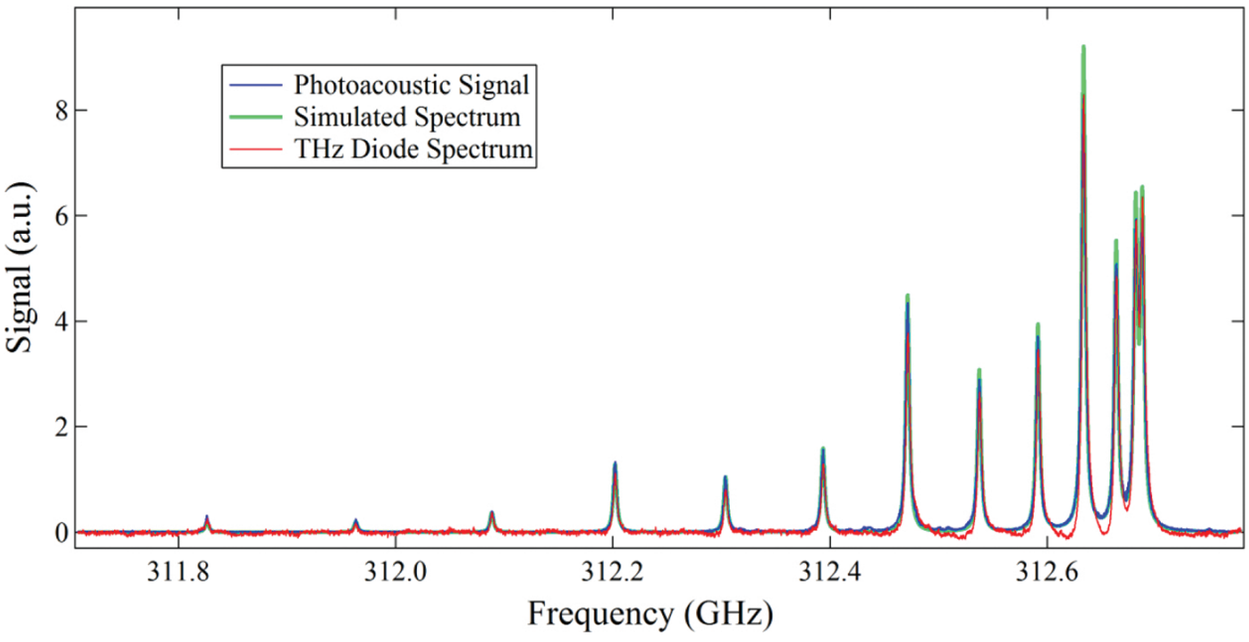

Figure 15. PA data and the simultaneously recorded THz diode signal are compared to the simulated absorption spectra of CH_3CN recorded at 13 mTorr.

With excellent PA spectral data collected at multiple low pressures, a further analysis of the system performance parameters was carried out. SNR, sensitivity, and NNEA coefficient of

http://dx.doi.org/10.5772/62571

the PA sensor were important figures of merit for system performance. Data collected at 13 mTorr with the THz source power attenuated down to ~0.1 mW had a peak PA signal of 7.084, measured at 312.6336 GHz. The RMS noise floor for the collected data set was determined to be 0.0058, which was located between two weak absorption peeks at 311.925 GHz. Using the peak and minimum PA signals in the spectral data collection, the SNR = 1221. Using Eqs. (2) and (3), a sensitivity of 1.97×10^{-5} cm^{-1} and an NNEA of 1.39×10^{-9} cm^{-1} W $Hz^{-½}$ were determined using a 0.5 s signal averaging time. The sensitivity and NNEA achieved in this effort were excellent and compare well to previously reported cantilever PA trace gas detection systems while operating at significantly lower chamber pressures.

6. Conclusions

In this work, a sensitive MEMS cantilever design was successfully modeled, fabricated, and tested in a custom-designed low-vacuum THz PA chemical sensing and molecular spectroscopy system. Cantilever design parameters of length, width, and thickness of the cantilever structure were used to select a cantilever design that was sensitive to the generated PA pressures in the chamber. With this novel system, the first ever cantilever-based THz PA spectrum was collected and analyzed at low chamber pressures in the 2 to 60 mTorr range. The pressure regimes tested here were several orders of magnitude lower than the trace gas detection cantilever PA systems discussed earlier [11–18]. Significant PA signals were achieved at chamber pressures as low as 2 mTorr. For THz spectroscopy applications, the sensor size and chamber pressures tested were also an order of magnitude smaller than the membrane sensor system used by Krupnov and Burenin [9]. By collecting PA spectra in the 2 mTorr pressure regime, it allowed for a primarily Doppler limited line broadening of the CH_3CN, making closely spaced absorption lines highly resolvable.

This research effort achieved an NNEA of 1.39×10^{-9} cm^{-1} W $Hz^{-½}$ using a compact THz PA spectroscopy and chemical sensing system. Due to its compact size, the system could be used as a portable chemical sensing and spectroscopy platform. This would be a great advantage in comparison to a large traditional absorption cell for spectroscopy applications and may lead one day to a handheld THz chemical sensor or MEMS detector arrays for THz imaging applications.

Acknowledgements

The authors thank the Air Force Office of Scientific Research (AFOSR) for funding this effort (F4FGA04013J001) and the Air Force Research Laboratory (AFRL) Sensors Directorate for their assistance. The authors also thank the AFIT clean-room staff, Mr. Richard Johnston, and Mr. Thomas Stevenson.

Author details

Nathan Glauvitz[1], Ronald A. Coutu[1*], Ivan R. Medvedev[2] and Douglas T. Petkie[2]

*Address all correspondence to: Ronald.Coutu@AFIT.edu

1 Air Force Institute of Technology, Hobson Way, Wright-Patterson AFB, USA

2 Wright State University, Dayton, USA

The views expressed in this paper are those of the authors and do not reflect the official policy or position of the United States Air Force, Department of Defense, or the U.S. Government.

References

[1] West G. A., Barrett J. J., Siebert D. R., and Reddy K. V. Photoacoustic spectroscopy. *Rev. Sci. Instrum. 54*, pp. 797–817, 1983.

[2] Bell A. G. *Upon the Production of Sound by Radiant Energy.* Washington, DC: Gibson Brothers Printers, 1881.

[3] Miklos A., Hess P., and Bozoki Z. Application of acoustic resonators in photoacoustic trace gas analysis and metrology. *Rev. Sci. Instrum. 72*, pp. 1937–1955, 2001.

[4] Brugel W. *An Introduction to Infrared Spectroscopy.* New York: John Wiley & Sons, Inc., 1962.

[5] Kosterev A. A., Bakhirkin Y. A., Curl R. F., and Tittel F. K. Quartz-enhanced photoacoustic spectroscopy. *Opt. Lett. 27*, pp. 1902–1904, 2002.

[6] Kosterev A. A., Tittel F. K., Serebryakov D. V., Malinovsky A. L., and Morozov I. V. Applications of quartz tuning forks in spectroscopic gas sensing. *Rev. Sci. Instrum. 76*, pp. 043105, 2005.

[7] Liu K., Li J., Wang L., Tan T., Zhang W., Gao X., Chen W., and Tittel F. K. Trace gas sensor based on quartz tuning fork enhanced laser photoacoustic spectroscopy. *Appl. Phys. B 94*, pp. 527–533, 2009.

[8] Borri S., Patimisco P., Sampaolo A., Beere H. E., Ritchie D. A., Vitiello M. S., Scamarcio G., and Spagnolo V. Terahertz quartz enhanced photo-acoustic sensor. *Appl. Phys. Lett. 103*, pp. 021105, 2013.

[9] Krupnov A. F. and Burenin A. V. New methods in submillimeter microwave spectroscopy. In *Molecular Spectroscopy: Modern Research*, Rao K. N., ed. New York: Academic Press, Inc., 1976, pp. 93–126.

[10] Firebaugh S. L., Jensen K. F., and Schmidt M. A. Miniaturization and integration of photoacoustic detection with a microfabricated chemical reactor system. *J. Microelectromech. Syst. 10*, pp. 232–237, 2001.

[11] Ledermann N., Muralt P., Baborowski J., Forster M., and Pellaux J. Piezoelectric pb(zrx, ti1-x)O_3 thin film cantilever and bridge acoustic sensors for miniaturized photoacoustic gas detectors. *J. Micromech. Microeng. 14*, pp. 1650–1658, 2004.

[12] Kuusela T., Peura J., Matveev B. A., Remennyy M. A., and Stus N. M. Photoacoustic gas detection using a cantilever microphone and III-V mid-IR LEDs. *Vibrat. Spectrosc. 51*, pp. 289–293, 2009.

[13] Kuusela T. and Kauppinen J. Photoacoustic gas analysis using interferometric cantilever microphone. *Appl. Spectrosc. Rev. 42*, pp. 443–474, 2007.

[14] McNaghten E., Grant K., Parkes A., and Martin P. Simultaneous detection of trace gases using multiplexed tunable diode lasers and a photoacoustic cell containing a cantilever microphone. *Appl. Phys. B Lasers Opt. 107*, pp. 861–871, 2012.

[15] Adamson B. D., Sader J. E., and Bieske E. J. Photoacoustic detection of gases using microcantilevers. *J. Appl. Phys. 106*, pp. 114510, 2009.

[16] Fonsen J., Koskinen V., Roth K., and Kauppinen J. Dual cantilever enhanced photoacoustic detector with pulsed broadband IR-source. *Vibrat. Spectrosc. 50*, pp. 214–217, 2009.

[17] Peltola J., Vainio M., Hieta T., Uotila J., Sinisalo S., Metsälä M., Siltanen M., and Halonen L. High sensitivity trace gas detection by cantilever-enhanced photoacoustic spectroscopy using a mid-infrared continuous-wave optical parametric oscillator. *Opt. Express 21(8)*, pp. 10240–10250, 2013.

[18] Kauppinen J., Wilcken K., Kauppinen I., and Koskinen V. High sensitivity in gas analysis with photoacoustic detection. *Microchem. J. 76*, pp. 151–159, 2004.

[19] Sievilä P., Chekurov N., Raittila J., and Tittonen I. Sensitivity-improved silicon cantilever microphone for acousto-optical detection. *Sens. Actuators A Phys. 190*, pp. 90–95, 2013.

[20] Koskinen V., Fonsen J., Roth K., and Kauppinen J. Progress in cantilever enhanced photoacoustic spectroscopy. *Vibrat. Spectrosc. 48*, pp. 16–21, 2008.

[21] Ariyoshi S., Otani C., Dobroiu A., Matsuo H., Sato H., Taino T., Kawase K., and Shimizu H. M., Superconducting detector array for terahertz imaging applications. *Jpn. J. Appl. Phys. 45*, pp. L1004–L1006, 2006.

[22] Tao H., Kadlec E. A., Strikwerda A. C., Fan K., Padilla W. J., Averitt R. D., Shaner E. A., and Zhang X. Microwave and terahertz wave sensing with metamaterials. *Opt. Express 19*, pp. 21620–21626, 2011.

[23] Chen S., Choe Y., Baumgartel L., Lin A., and Kim E. S. Edge-released, piezoelectric MEMS acoustic transducers in array configuration. *J. Micromech. Microeng. 22*, pp. 025005, 2012.

[24] Blom F. R., Bouwstra S., Elwenspoek M., and Fluitman J. H. J. Dependence of the quality factor of micromachined silicon beam resonators on pressure and geometry. *J. Vac. Sci. Technol. B 10*, pp. 19–26, 1992.

[25] Uotila J., Koskinen V., and Kauppinen J. Selective differential photoacoustic method for trace gas analysis. *Vibrat. Spectrosc. 38*, pp. 3–9, 2005.

[26] Glauvitz N. E., Coutu R. A., Kistler M., Medvedev I. R., and Petkie D. T. MEMS cantilever sensor for photoacoustic detection of terahertz radiation. In *Proceeding of SEM 2013 Annual Conference & Exposition on Experimental and Applied Mechanics*, Lombard, IL, 2013.

[27] Wang Y., Lee C., and Chiang C. A MEMS-based air flow sensor with a free-standing micro-cantilever structure. *Sensors 7*, pp. 2389–2401, 2007.

[28] Garcia-Valenzuela A. and Villatoro J. Noise in optical measurements of cantilever deflections. *J. Appl. Phys. 84*, pp. 58–63, 1998.